ELSEVIER

Earth and Planetary Science Letters 199 (2002) 373–388

EPSL

www.elsevier.com/locate/epsl

Numerical models of crustal scale convection and partial melting beneath the Altiplano–Puna plateau

A.Yu. Babeyko [a,b], S.V. Sobolev [a,*], R.B. Trumbull [a], O. Oncken [a], L.L. Lavier [a,c]

[a] *GeoForschungsZentrum, Telegrafenberg, 14473 Potsdam, Germany*
[b] *Institute of Physics of the Earth, B. Gruzinskaya 10, 123810 Moscow, Russia*
[c] *California Institute of Technology, Seismological Laboratory 252-21, Pasadena, CA 91125, USA*

Received 28 March 2001; received in revised form 1 October 2001; accepted 11 March 2002

Abstract

We employ 2-D thermo-mechanical modelling to study possible mechanisms for generating large-scale crustal magmas in the Altiplano–Puna region of the Central Andes. The peak of ignimbrite activity in the late Miocene and Pliocene is associated in space and time with tectonic shortening and plateau uplift. A seismic low-velocity zone and other geophysical observations indicate that partial melting in the mid-crust is still present under the ignimbrite province today. We show that neither radiogenic heat production in a thickening crust, nor shear heating due to tectonic shortening, nor heat brought by intrusions of arc magmas into the mid-crust can heat the mid-crust to the degree and within the time frame suggested by the geologic, petrologic and geophysical observations. A viable mechanism to achieve high temperatures within the time constraints is convective heat and mass transfer by partially molten lower crust which itself was heated by enhanced mantle heat flow, possibly associated with delamination of the mantle lithosphere during tectonic shortening and intensified magmatic arc activity. The thermo-mechanical models explain the mid-crustal low-velocity zone and the high and strongly variable surface heat flow observed in the Altiplano. Convection by bulk flow of the crust appears when the middle and lower crust are mechanically weak (quartz-dominated rheology), the basal heat flow from the mantle is high (>60 mW/m^2) and tectonic shortening is active. We argue that these conditions are satisfied in the Central Andes orogen.

Keywords: numerical models; melting; plate collision; Andes; convection

1. Introduction

The peak phase of compressive deformation and uplift of the Central Andes in the Miocene and Pliocene (<25 Ma [1,2]) overlaps in time with a major phase of felsic magmatism in the region, evidenced by the existence of one of the largest Neogene ignimbrite provinces in the world. The dacitic ignimbrites erupted from caldera complexes located in and to the east of the present arc (Fig. 1). The greatest concentration of ignimbrites, with over 10^4 km^3 erupted volume, makes up the Altiplano–Puna Volcanic Complex

* Corresponding author.
Tel.: +49-331-288-1248; Fax: +49-331-288-1266.
E-mail address: stephan@gfz-potsdam.de (S.V. Sobolev).

0012-821X/02/$ – see front matter
PII: S0012-821X(02)00597-6

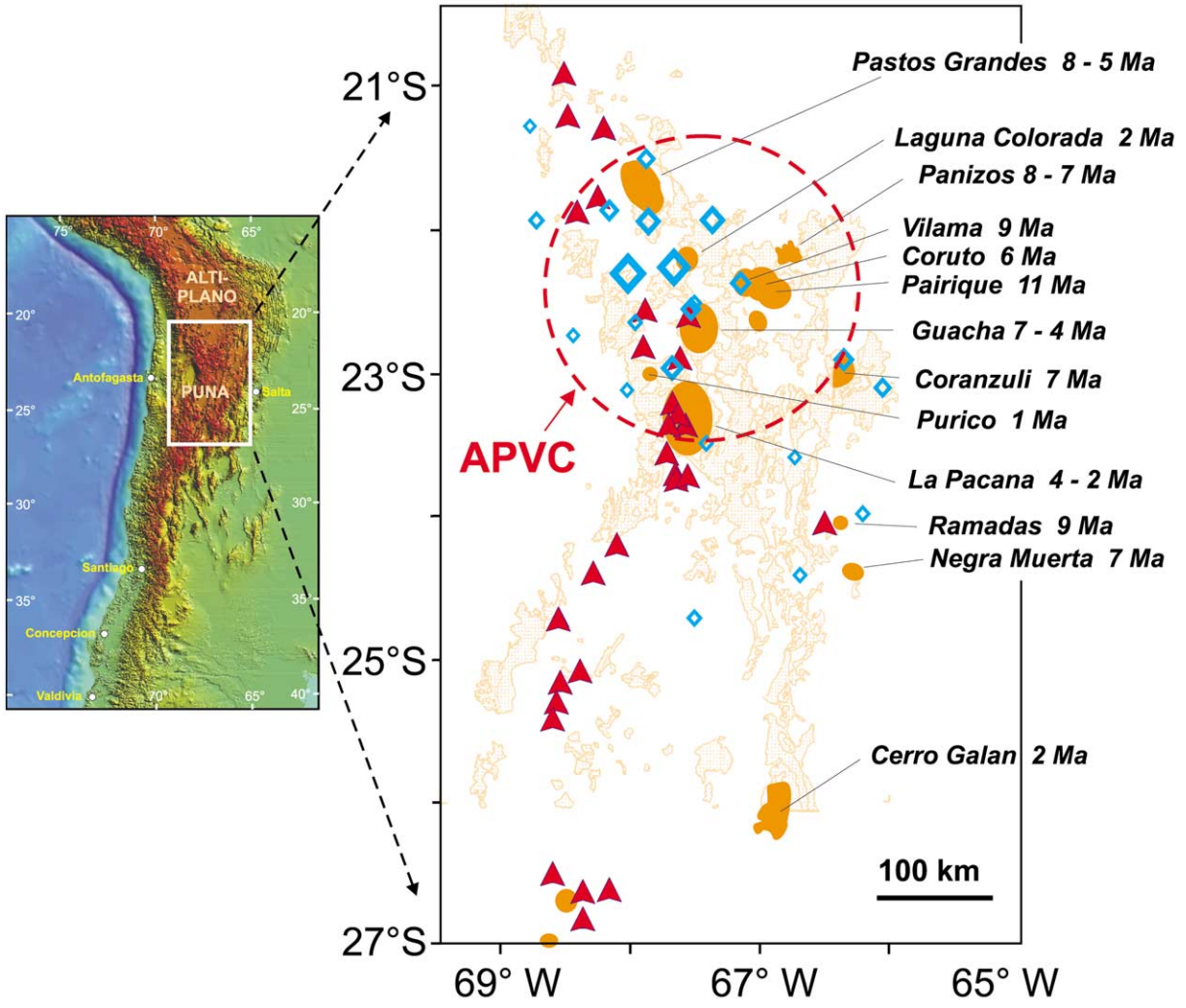

Fig. 1. Location map of the study region with the distribution of active arc volcanoes (red triangles) and location of major ignimbrite calderas (reddish domains) and flows (light reddish fields) of the Miocene–Pliocene ignimbrite province APVC [3]. The caldera ages are compiled from [2–6]. Also shown are seismic stations which recorded significant P–S conversions from the mid-crustal low-velocity zone (blue diamonds indicate station locations, symbol size is proportional to conversion amplitude) from [8]. Note the correspondence of strongest P–S conversions with the area of the APVC.

(APVC) [3]. Geochemical and isotopic studies suggest that the ignimbrite magmas from the large caldera centers are well-mixed hybrids of crustal melts and mafic arc magma [4–7]. The proportion of mafic components in the hybrid magmas is not well constrained and estimates range from about one-third [7] to one-half [5], depending on assumptions made about the endmember compositions.

The comparatively sudden onset of ignimbrite activity in the late Miocene is a first-order feature of the Central Andean arc and it reflects a marked change in the thermal state of the crust which likely persists today. Ignimbrite activity has waned since the Pliocene but geophysical data suggest an anomalously hot and partially molten middle crust beneath the Altiplano–Puna Plateau and the Western Cordillera. Yuan et al. [8] docu-

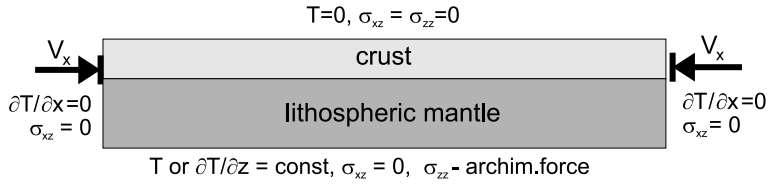

Fig. 2. Sketch showing the general geometry and boundary conditions of the starting model.

mented a prominent mid-crustal zone of low seismic velocity (Andean Low Velocity Zone = ALVZ) with its top at about 20 km depth. The ALVZ extends across the entire plateau but the most pronounced part of it corresponds with the APVC and is thought to reflect crustal melting [8,9]. Pre-eruptive temperatures for APVC ignimbrite magmas have been estimated at 700–800°C [7,10]; thus peak temperatures in the source region were at least 800°C. The inference of extensive melting at the mid-crustal level beneath the Western Cordillera is also consistent with wide-angle seismic, gravity and electromagnetic data [11,12], high surface heat flow [13] and high average V_p/V_s ratio in the crust [8,14].

The aim of this study is to use coupled thermo-mechanical modelling to investigate the cause of crustal heating and melting in the Central Andes and explore its relationship with tectonic shortening and plateau formation. The focus is on the APVC region (21–24°S) because good petrologic and geophysical datasets exist and because this area saw the peak of ignimbrite magmatism. The geophysical and petrologic evidence suggests that magma source region(s) with temperatures above 800°C are located within a laterally extensive but internally heterogeneous zone at some 20–25 km depth in the crust. A critical aspect of the modelling is the question of timing. The age of ignimbrite activity in the APVC indicates that the anomalous thermal structure of the crust in the region was established by at least 10 Ma. The timing of tectonic shortening is less definitive. Plate convergence and subduction have been ongoing since the Triassic, but compressional deformation in the Central Andes only began in Eocene times [15] with minor deformation at the margins of the future plateau. Deformation accelerated at some 29–25 Ma, a time that correlates with an increase in plate convergence rate [2], and this caused a subsequent near-doubling of crustal thickness. For the modelling, we therefore choose 30–25 Ma as the time when shortening starts, but also discuss the effect of other timescales on the model results. According to these constraints, heating and partial melting of the middle crust was achieved within some 10–20 Myr after initiation of intensive tectonic shortening. Possible mechanisms of crustal heating which are considered include: (i) enhanced radiogenic heating due to the crustal thickening [16,17], (ii) shear heating caused by active deformation [18–20], (iii) heating by intrusion and cooling of arc andesites [21], and (iv) heating as a result of increased mantle heat flow due to asthenospheric upwelling [22–24].

2. Modelling technique and approach

The numerical modelling was done using the modified finite-difference/finite-element thermo-mechanical code PARAVOZ by Polyakov and Podladchikov [25], which implements the FLAC algorithm of Cundall [26]. An explicit, time-marching calculation scheme allows any combination of nonlinear rheologies and has proved to be very effective for geodynamic modelling in a number of applications (e.g., [27–29]). The original code was modified in this study to allow more stable calculation of large deformation (new remeshing algorithm), to include additional options (e.g., shear heating, melting, melt removal and emplacement) and to perform parallel computing. The Appendix gives detailed descriptions of the method and results of benchmark testing and calibration.

The general model description used for our calculations is illustrated in Fig. 2. The 130 km thick lithosphere in the initial stage consists of a 35 km thick crust with quartz-dominated rheology and a

95 km mantle layer with olivine-dominated rheology. The corresponding material parameters are listed in Table 1. At each calculation step the algorithm automatically selects a rheology (elasto-plastic or nonlinear visco-elastic) that is more appropriate at the current conditions of temperature, strain rate, etc. The initial temperature distribution corresponds to a steady state continental geotherm with 700°C at the base of the crust. Values chosen for heat-producing elements U, Th and K in the crust are from an extensive compilation of Central Andes basement data [33]. Shortening in the model occurs with fixed boundary velocities corresponding to a typical Andean strain rate of 10^{-15} s^{-1} (equivalent to crustal doubling in ca. 30 Myr). The temperature at the base of the model lithosphere is fixed at $T_a = 1300$°C.

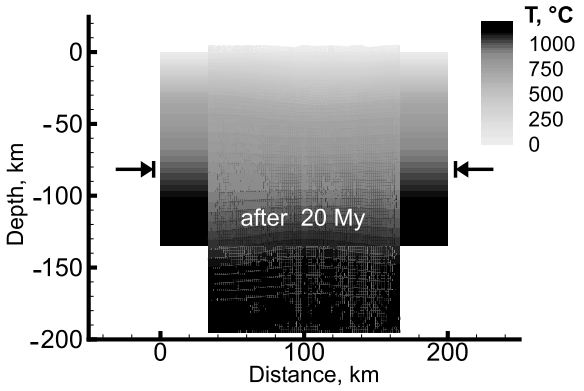

Fig. 3. Model results showing the temperature evolution of tectonically thickened lithosphere, taking only internal heat sources (radiogenic and shear heating) into account (Model I-a). Note that in this case the mid-crust becomes colder with time.

3. Modelling results

3.1. Intra-crustal heat sources: radiogenic and shear heating

It is well established that the thermal effect of burial of a heat-producing crust can be significant after several tens of million years [17,34], or even faster in a case of accretion of heat-productive crust above a subducted continental plate [16]. Previous studies have also shown that the effect of shear or dissipative heating can be significant if both stress and strain rate are high [19,20].

Fig. 3 presents the calculated 2-D temperature field in the model after 20 Myr of shortening, taking both radiogenic and shear heating into account according to the parameter choices in Table 1. The time evolution of the average temperature for the depth interval 20–25 km is shown in Fig. 6a by the line labelled I-a. Both diagrams show that the middle crust actually becomes cold-

Table 1
Rheological and thermal parameters used in the modelling

Parameter	Felsic crust		Mantle peridotite
	weak	strong	
ρ, density at 20°C, 1 bar, kg/m^3	2700*		3300*
α, thermal expansion, K^{-1}	3.7×10^{-5}*		3.0×10^{-5}*
K, G, elastic moduli, GPa	55, 36*		122, 74*
C_p, heat capacity, J/kg/K	1200*		1200*
λ, heat conductivity, W/K/m	$0.38\times\ln(T[°C])+4.06$**		3.3
A, heat productivity, μW/m^3	1.3 for upper crust ($z<20$ km at $t=0$); 0.85 for lower crust##		0
B, pre-exponential multiplier, GPa^{-n} s^{-1}	100#	100#	4×10^{15}#
E_a, activation energy, J/mol	1.37×10^{5}#	1.56×10^{5}#	5.4×10^{5}#
n, power-law exponent	1.9#	2.4#	3.5#
Mohr–Coloumb elasto-plasticity with softening	friction angle 30°; dilation 0°; cohesion 40 MPa, linear decrease of cohesion to 4 MPa at 10% strain		
Crustal melt parameters	heat of fusion 4.2×10^5 J/kg, melt density 2430 kg/m^3		

*[30]; weak-crust parameters as for wet granite in compilation by Ranalli and Murphy [31], strong-crust as for their quartzite, and mantle peridotite as for their olivine; **[32]; [33].

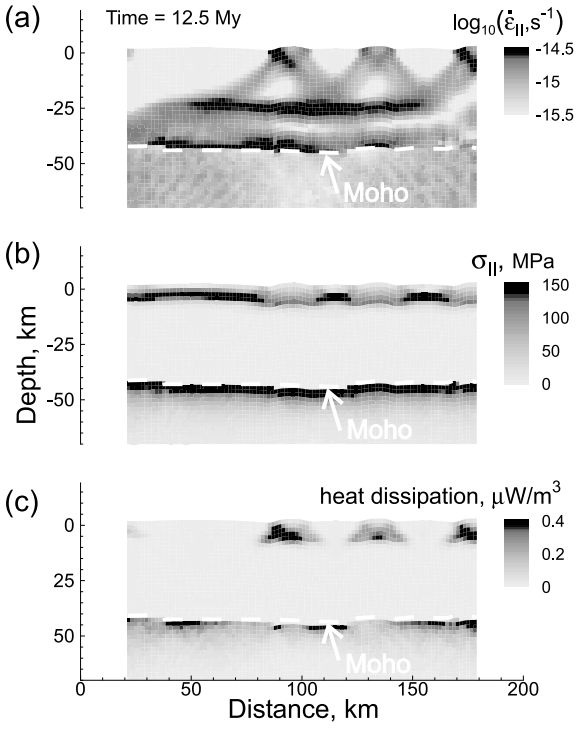

Fig. 4. Heat production due to energy dissipation in deformed (shortened) lithosphere (Model I-a). (a) Depth distribution of the second invariant of the strain rate deviator. (b) Depth distribution of the second invariant of the stress deviator. (c) Heat production due to dissipation, which is the product of the two fields shown in panels a and b.

er with time during shortening. This happens because shortening produces a net downward movement of colder material and this effect overwhelms the heat produced from internal sources. Although the concentration of radioactive elements in the crust per unit surface area increases due to crustal thickening, the overall effect of radiogenic heating at 20–25 km depth after 15 Myr of shortening does not exceed a few tens of degrees. The effect of the shear heating is even less important. Strain localization in the model confines high strain rates to places where deformation is easiest (low stresses) and therefore shear heating, which is the product of stress and strain rate, remains moderate. This is demonstrated in Fig. 4, which shows the depth distribution of the second invariants of strain rate and stress deviators. High strain rates are associated with 'fault zones' in the upper and middle crust and with a region of lower crustal flow (Fig. 4a). High stresses occur outside the fault zones in the upper crust and in the uppermost mantle (Fig. 4b). Shear heating is relatively high within fault zones in the brittle upper crust and in the mantle just below the Moho, but even in those places heat production due to shear is smaller than radiogenic heat production (Fig. 4c).

3.2. Effect of direct magma intrusions

The idea that widespread partial melting in the thickened Central Andes crust is due to heating from intruded arc magmas was originally suggested for the APVC volcanism in [3] and thermal aspects of the process were examined by numerical modelling [21]. Our modelling differs from the latter study because we include the effects of active deformation and internal heating discussed above, and we treat the thermal effect of intrusion as the integral result of many discrete magma batches distributed in space and time.

To calculate the thermal effect of magma intrusions into the middle crust we consider the following model. Magma is emplaced into a layer of the crust between 20 and 25 km depth as discrete intrusions which are distributed randomly in time and space such that the overall magma flux (volume of magma per km and Myr) meets a prescribed value. The intrusions have dimensions guided by a compilation of observed pluton dimensions [35]. Their lengths varied from 0.5 to 5 km and the thicknesses varied from 50 to 500 m. The zone into which intrusions are emplaced is 100 km wide, corresponding roughly to the lateral extent of the APVC calderas (Fig. 1). The magma is assigned a temperature of 1200°C, which is generous considering that erupted andesites in the region record magma temperatures of 900–1100°C [36–38]. The overall magma flux in the intruded zone is one of the model variables. Francis and Hawkesworth [39] estimated the magma productivity in the Central Andes arc at 4–8 km^3/Myr/km arc length. Global estimates from island arcs are much greater than this, from around 30 km^3/Myr/km arc [40] to about twice that value [41].

The effects of cooling and solidification of the

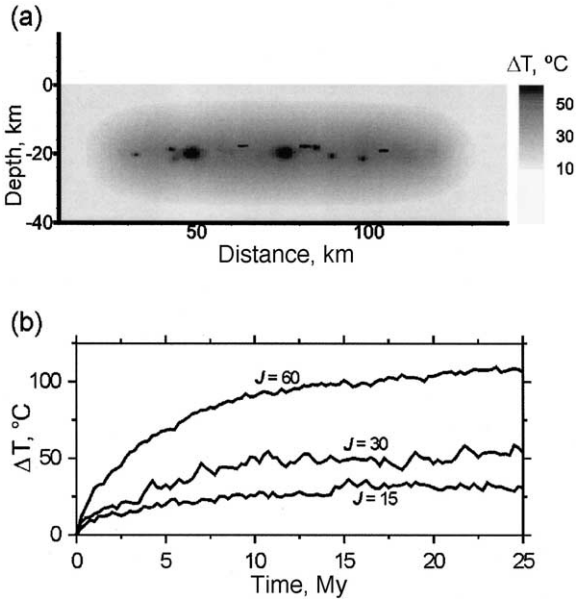

Fig. 5. The thermal effect of intruding arc magma into the mid-crust (Model I-b). (a) Differential temperature (current temperature minus initial temperature) in the crust at $t = 12$ Myr calculated for a magma flux into the mid-crust of 30 km^3/Myr/km of arc length. Note that intrusions can significantly heat the crust only locally and for a short time. (b) Increase of average temperature at 20–25 km depth calculated for magma fluxes of 15, 30 and 60 km^3/Myr/km arc.

intrusions are calculated using the thermal parameters listed in Table 1. Fig. 5a shows a snapshot of the differential temperature distribution (temperature minus initial temperature) from one of the numerical experiments at $t = 12$ Myr. In this particular model the magma flux was 30 km^3/Myr/km arc. Fig. 5b shows the variation of average temperature at 20–25 km depth due to different magma fluxes. It is clear that even a magma flux of 60 km^3/Myr/km arc, which corresponds to a maximum arc productivity intruding the mid-crust, causes the average temperature of the intruded layer to increase by not more than 100°C. This is due to the efficient cooling of intrusions in the relatively shallow crust.

The line labelled I-b in Fig. 6a shows that the sum effect of random intrusion of arc magmas in the mid-crust (30 km^3/Myr/km arc) and internal heating are not sufficient to overcome the cooling effect caused by downward movement of cold material during shortening. Thus our numerical experiments suggest that neither heat production in the thickening crust, nor shear heating due to deformation, nor intrusion of arc magmas can produce widespread partial melting in the mid-crust of the Altiplano–Puna plateau within the time constraints, parameter values and model scenarios considered.

3.3. Increased mantle heat flow

The alternative possibility to produce high temperatures in the mid-crust is to increase the basal heat flow from the mantle and to transport this heat effectively upward. Processes which could increase mantle heat flow in this setting include: (1)

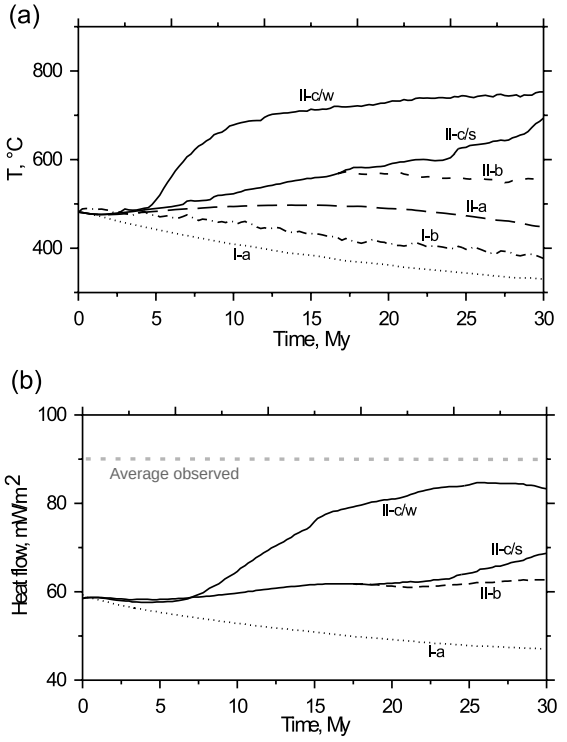

Fig. 6. (a) Evolution of the average temperature at 20–25 km depth for the different model scenarios discussed in the text. Curves are labeled according to model numbers keyed to text. For model II-c both cases of 'weak' (line II-c/w) and 'strong' (II-c/s) rheologies are shown. (b) Calculated surface heat flow for the model scenarios. The dotted line shows the average heat flow observed in the Western Cordillera and Altiplano [13].

enhanced arc productivity due to higher convergence rates and volatile flux to the mantle wedge, (2) delamination of relatively cool mantle lithosphere replaced by hotter asthenosphere [1,22–24], or (3) steepening of the down-going plate and consequent inflow of asthenosphere [1,2].

In this series of models we consider a single-layered 35 km thick crust being shortened at a constant strain rate of 10^{-15} s^{-1}. The crust is underlain by a thin (3 km) stabilizing layer with zero shear stress and mantle thermal properties which is needed to prevent deformation instability at the lower boundary. At some initial time, the basal heat flow at the model bottom is increased to a prescribed value and then held constant (results for 60 mW/m^2 are shown below). If the temperature at the base of the sub-crustal layer reaches 1200°C, this temperature is used instead of a constant heat flow as the thermal boundary condition. One series of calculations (Model II-a) represents the endmember case where heat transport is entirely conductive. However, when temperatures in the lower crust become high enough, processes occur which enable more efficient heat transfer. These processes, which are the main focus of the modelling, include: (i) partial melting, (ii) melt segregation and removal, followed by intrusion into the upper/middle crust, (iii) bulk flow (convection) of the hot and partially molten lower crust. In the following sections we discuss the above processes in a series of models. For simplicity, the Moho heat flow was increased at the same time as the shortening started. The calculations also include the effects of internal heat sources as described in Section 3.1.

Partial melting is modelled using the relationships between melt fraction and temperature determined in experiments on vapor-free melting of felsic muscovite–biotite and biotite gneisses [42]. Melt accumulation and removal is modelled following the concept of percolation thresholds [43,44]. Melt leaves the rock matrix when its fraction exceeds the second percolation threshold. Extracted melt in our model is then assumed to intrude completely into the 20–25 km depth level and this process continues until the melt fraction in the lower crustal reservoir falls below the first percolation threshold. At some stage, heating and partial melting in the lower crust can cause the lowermost layer to become gravitationally unstable (Rayleigh–Taylor instability) and to initiate intra-crustal convection. This process occurs readily in our models if a low viscosity for the lower crust is adopted (see below).

3.3.1. *Pure thermal conductivity (Model II-a)*

In the first model the lower crust is neither allowed to melt nor to convect. This is achieved by assigning to it a high solidus temperature (1300°C) and high viscosity (10^{21} Pa s). When the mantle heat flow is increased to 60 mW/m^2, calculations show that the combined effect of internal heat sources and increased mantle heat flow in this model just balance the effect of cooling from downward movement of material due to shortening (line II-a in Fig. 6a). After 25–30 Myr of shortening and heating, the average temperature at 20–25 km depth remains below 500°C.

3.3.2. *Partial melting with melt segregation and removal (Model II-b)*

In this model we exclude convection of bulk crustal material (by assigning a high viscosity to the lower crust), but melting occurs when the vapor-absent solidus of biotite gneiss, according to [42], is exceeded. Melt segregates and is transported to the mid-crust as described above when the melt fraction exceeds the second percolation threshold (first and second percolations threshold are 10% and 25%, respectively). Again, the Moho heat flow is increased to 60 mW/m^2 at $t=0$. In this model the lower crust starts to melt after 1 Myr and the first segregation occurs at $t \sim 2.5$ Myr. The average temperature in the mid-crust rises to 580°C at 17 Myr and then slowly decreases (Fig. 6a, line II-b).

3.3.3. *Crustal convection with partial melting and melt segregation (Model II-c)*

The last model differs from the previous one in that we now allow crustal convection to occur. The model assumes that the entire crust has rheological properties controlled by quartz (see Table 1). We consider two different crustal rheologies, one relatively weak, corresponding to wet granite, and another relatively strong, correspond-

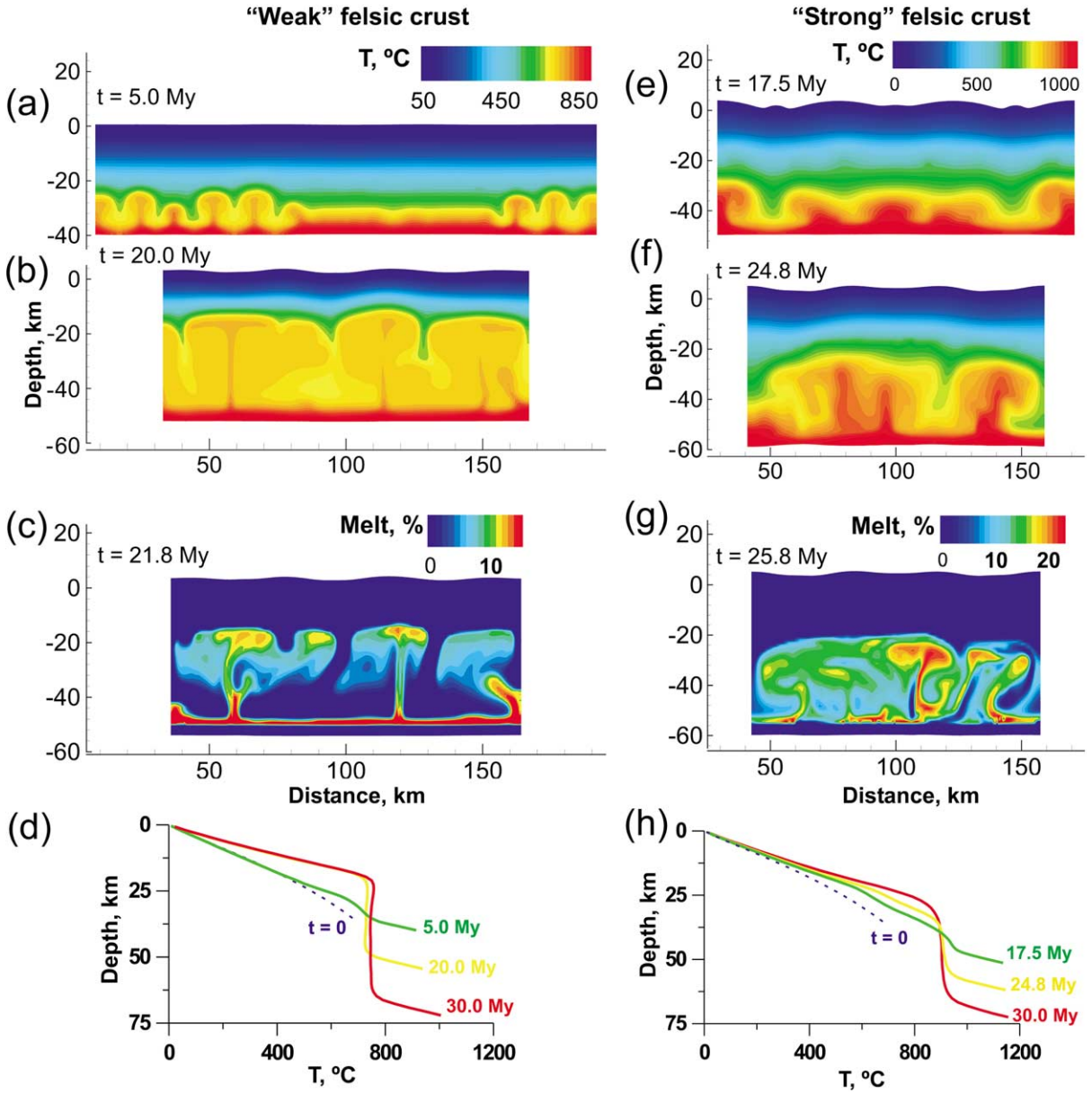

Fig. 7. Intra-crustal convection resulting from enhanced mantle heat flow (Model II-c). Shown are series of snapshots at different times after inception of shortening and enhanced mantle heat flow: panels a and b are temperature distributions at initial (a) and mature (b) stages of convection for 'weak' crustal rheology, panel c shows melt fraction distribution at mature stage of convection and panel d average temperature–depth dependences at different times for 'weak' crustal rheology. Panels e–h are the same as panels a–d but for 'strong' crustal rheology.

ing to dry quartzite, both from the compilation by Ranalli and Murphy [31]. Viscosities of these two examples differ by almost two orders of magnitude. In the experiments with weak rheology we model the melting behavior of muscovite-biotite gneiss and in experiments with stronger rheology we use biotite-gneiss behavior (both from [42]). During the first 5 Myr this thermo-mechanical

model behaves exactly like the previous one for both crustal rheologies, but then the lowermost crust becomes unstable and convection may start. The evolution of convection is shown in Fig. 7 as temperature snapshots at different times, with the left and right panels representing cases for weak and strong crust, respectively. In weak crust, convection starts at about 5 Myr and passes rapidly to a stage in which small and narrow jets of rising material merge to create larger plumes. In this first stage, temperatures at 20–25 km depth increase to 700°C on average and above 800°C locally, depending on the flow pattern (Fig. 6a, line II-c/w). After some 10–15 Myr the convection pattern becomes more stable, with hot material flowing upward through a few narrow channels to a depth of about 20 km where it then spreads laterally. Material flux through the channels pulsates and the number of channels active at any one time may also change. The average temperature in the 20–25 km depth range at this stage is 700–750°C and local maxima exceed 800°C. In the case of a rheologically stronger and chemically less fertile crust, convection starts some 10 Myr later and develops more slowly (see also Fig. 6a, line II-c/s). High temperatures at the mid-crustal level develop after some 20 Myr and the quasi-stable configuration is reached after 25 Myr. From the very beginning, the pattern of convection is coarser compared to the case of weak and fertile crust. Note that, if the crust is hot from the very beginning and/or basal heat flow is much higher than 60 mW/m^2 (e.g., due to massive basaltic underplating), then patterns of crustal convection similar to those in Fig. 7 can be produced within a much shorter timespan of 1–2 Myr [45].

To summarize the results for increased basal heat flow, the curves in Fig. 6a show that only the model for heat convection (II-c) is capable of achieving melting temperatures in the mid-crust which are needed to satisfy the geophysical and petrologic constraints. Fig. 6b shows the calculated surface heat flow for each of the models together with the observed values from the Altiplano and Western Cordillera [13]. Again, only the convection model (II-c) predicts average surface heat flow values, at about 80 mW/m^2, close to the observed average. Note that the calculated heat flow is a lower bound because we do not consider heat transport by movement of magma through the upper crust, which of course is the case for a volcanic province like the APVC. A characteristic feature of the observed surface heat flow data is its large spatial variability [13], which is precisely what our convection models predict (see Fig. 7). Note also that earlier thermal models based on solution of the conductive thermal equation [46] were not able to fit the measured high surface heat flow and its spatial variability.

As explained in the Appendix, the explicit pseudo-inertial algorithm we use tends to slow the most rapid processes in the models, one of which is material flow within growing plumes. Moreover, due to computation difficulties we had to limit the minimal viscosity in the models to 10^{17} Pa s, which is much higher than expected for high-degree partially molten rocks. Both of these effects cause the models to underestimate the speed of convection and therefore our results for convection models should be considered as conservative.

4. Discussion

4.1. Robustness of key results

We have shown above that intra-crustal heat production and large-scale intrusion of arc magmas are not sufficient to explain rapid heating in the mid-crust of the Central Andes and that increased basal heat flow with convective transport through the crust must be invoked. This statement is true within the framework of the modelling scenarios and parameters considered but we must enquire whether reasonable modification of the parameters and scenarios would change the conclusion. To address this question we have run a series of additional numerical experiments. The initial radiogenic heat production in the crust used in our model is already quite high (the crustal contribution to the steady state surface heat flow is 40 mW/m^2), but we ran a further experiment with 50% higher radiogenic heat production, other parameters being unchanged. In this new

experiment, the initial temperature at the 20–25 km depth interval is 50° higher than in previous experiments (540° vs. 490°C) and, as before, temperature decreases during shortening which is contrary to observations. An upper bound of the shear-heating effect was calculated by assuming that all heat dissipated by deformation is released within the 20–25 km depth interval. Even in this extreme scenario the average temperature at the target depth increased by only a few tens of degrees compared with previous runs (e.g., 40°C higher after 20 Myr shortening).

Finally, because the onset and duration of shortening in the Central Andes can be debated, we ran an experiment which violates the time constraints previously imposed and simulates a case where crustal shortening begins much earlier than the 25–30 Ma suggested by most workers [2]. In this experiment we shorten the lithosphere by 1.7 times over 25 Myr and then continue to monitor how temperature develops during thermal equilibration. Other conditions are the same as in Model I-a except that the lithosphere is not allowed to subside below 120 km. The result is that average temperatures at 20–25 km depth decrease during shortening as in Model I-a, but then gradually rise due to internal heat production, reaching 530°C 50 Myr after the end of shortening and a steady state temperature of 600°C after 200 Myr. If shortening continues beyond the 25 Myr duration considered in the new experiment, temperatures in the mid-crust will be lower than those given because the cooling phase associated with shortening will be prolonged. In the lower crust, partial melting begins after 15 Myr (i.e., 40 Myr after the onset of shortening) and conditions appropriate for convection assuming 'weak' rheology (Table 1) are established after some 40–50 Myr (about 70 Myr after shortening begins). Therefore, in combination with melting and heat advection from the lower crust, tectonic shortening could produce regional partial melting of the mid-crust without increased mantle heat flow, but only after several tens of Myr following the cessation of crustal thickening in that region. This conclusion does not depend on the mode of tectonic shortening (pure or simple shear) and it is inconsistent with geologic constraints from the Altiplano–Puna where crustal thickening and crustal melting overlap in time and space.

Therefore, based on the modelling results including tests of additional, more extreme scenarios, we are confident in concluding that crustal heat sources and magma intrusion cannot produce widespread melting in the mid-crust of the Altiplano–Puna region and that additional heat from the mantle is required. Processes which could cause an increased mantle heat flow include enhanced underplating of basaltic magma due to increased arc productivity and lithospheric thinning due to either delamination of relatively cool mantle lithosphere or steepening/retreat of the slab. However, the modelling has also shown that it is not enough to increase the heat flow from the mantle if heat is transferred only by thermal conduction mechanisms (see curve II-a in Fig. 6a). Instead, the additional heat must be advected into the mid-crust. Our modelling of the two mechanisms for this, i.e., heat transport by the melt phase after segregation (Model II-b) and bulk convection of partially molten lower crust (Model II-c), clearly suggests that only the bulk convection mechanism is viable (Fig. 6). The precise style of such convection is not entirely clear, and due to technical limitations we cannot yet model the process in its full complexity. Several potentially important factors not yet considered include the dramatic drop of viscosity in partially-molten crust, compositional heterogeneity in the crust, and mineral reactions due to partial melting and changes in temperature and pressure. The most critical point is the possibility of compositional gradients in the crust leading to an increase of density with depth. Under certain conditions such gradients can prevent bulk convection. However, other important cases of compositional gradients like lithological interlayering [47] or mafic intrusions in a felsic crust may even promote convection. For example, if partially molten, low-viscosity crust contains more refractory and denser mafic bodies, these may sink, increasing the buoyancy of the remainder. We would also note that there is petrological [33,48] and geophysical [14] evidence that most of the crust beneath the Altiplano–Puna is rather homogeneous and felsic in composition. Despite exist-

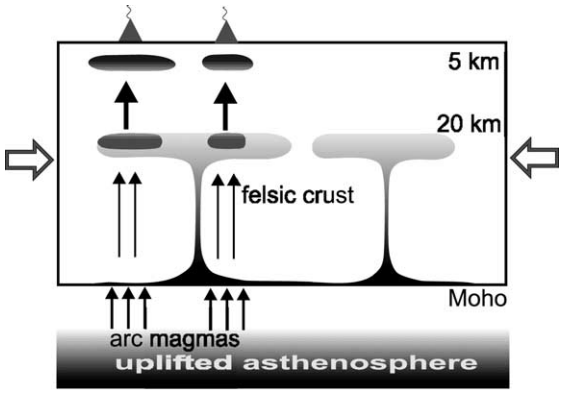

Fig. 8. Cartoon illustrating our preferred model for the Altiplano–Puna crust. Shading in the crust outlines the domains with partial melt and the density of shading increases with relative melt fraction.

ing limitations and the need for further refinements, our modelling suggests that bulk convection of partially molten lower crust can be very efficient in heat transport from the mantle into the mid-crust.

4.2. Preferred scenario

The preferred mechanism for achieving high temperatures and partial melting in the mid-crust of the Central Andes is an increased mantle heat flow combined with heat advection into the mid-crust caused by bulk convection of hot, partially molten lower crustal material and augmented by intrusion of the segregated melt. This mechanism produces high mid-crustal temperatures within 10–20 Myr after initiation of shortening (Fig. 6a) and satisfies the petrologic and age constraints on ignimbrite activity in the APVC. The convection models predict a top of the high-temperature zone at about 20 km depth (Fig. 7), a range of temperatures reaching 800°C and a spatial heterogeneity of temperature and surface heat flow, all of which are in good agreement with observations. The model predicts that a near-stationary stage of intra-crustal convection is achieved with a rather stable pattern of upwelling hot material (although material flux is fluctuating). This could be one explanation for the long-lived history of some major ignimbrite caldera complexes like La Pacana, where volcanic activity extended, with interruptions, for about 3 Myr [3]. Our modelling suggests that partially molten lower crustal material is likely advected into the mid-crust through narrow channels and then spreads laterally (Fig. 7b,c). Note that this pattern should in fact be even more pronounced than in Fig. 7 because of the damping effect of the most rapid flows due to the modelling method (see Appendix). The large-scale pattern produced by this mechanism, shown schematically in Fig. 8, is consistent with the location and intensity of the seismic low-velocity zone in the Central Andes [8,9].

Our numerical experiments suggest several conditions which appear necessary to initiate and support intra-crustal convection: (i) ongoing tectonic shortening, (ii) mantle heat flow of about 60 mW/m^2 or higher, (iii) quartz-dominated rheology in the crust. Here, we present a brief discussion justifying these conditions in the case of the Central Andes. The condition of ongoing shortening is appropriate for the Central Andes since the South American and Nazca plate convergence rate has been high since the Late Oligocene, when shortening began [2]. High mantle heat flow in the Central Andes could be related to this enhanced convergence rate due to an increase in magma productivity [3]. Another factor favoring higher mantle heat flow is slab steepening, and there is some suggestion based on the time/space distribution of volcanism in the Altiplano–Puna region that this occurred in the Miocene [2]. A more effective process, which goes hand-in-hand with tectonic shortening, is mantle lithosphere delamination and influx of hot asthenosphere. In this scenario, the highest mantle heat flow may be expected close to the magmatic arc, where the thermal effects of delaminated lithosphere and arc magmatism are combined. The condition that the entire crust be dominated rheologically by quartz is reasonable for the Central Andes although it may not be common globally. Quartz may dominate rock rheology if its proportion exceeds 10–20% [49]. The quartz content of the most common basement lithologies in the Altiplano upper and middle crust is greater than 30% and this may also be the case in the lower crust, since lower crustal xenoliths from the region, although

rare, are dominated by felsic granulites [33,48]. Furthermore, a new analysis of topography and crustal thickness in the Central Andes [14] concludes that the upper 50 km of the crust must be rather felsic.

As a final point, although we can conclude that the combination of the high mantle heat flow, intra-crustal convection and melt segregation from the lower crust is necessary and sufficient to explain mid-crustal temperatures beneath the APVC region, we recognize the spatial relationship of the APVC with the active arc (Fig. 1) and the fact that the ignimbrites are hybrid magmas [5,7,10]. Most likely, arc magmatism contributed to large-scale crustal melting in this region by contributing to increased basal heat flow from magmatic underplating and by input of heat and fluid into the middle crust via andesitic intrusions. Also, heat and fluid input from the arc may significantly decrease the viscosity of the crust, thus promoting crustal convection. It may be that the regional concentration and longevity of crustal magmatism in the APVC is due to the combined effect of lithospheric delamination with the active arc in this location.

According to our preferred model, which is illustrated in Fig. 8, the onset of tectonic shortening and an increase of basal heat flow (possibly due to asthenospheric upwelling and magmatic underplating) some 25–30 Myr ago promoted lower crustal convection. That led to a temperature increase in the mid-crust up to 700–800°C within 10–20 Myr. The rheology and density of this hot zone, once established, slowed the ascent of arc magmas. As these magmas became increasingly trapped and mixed with crustal melts, their heat and volatile contents would intensify the degree of crustal melting and perhaps also promote transport of the hybrid, felsic magmas to near-surface chambers from which they erupted as ignimbrites.

5. Conclusions

The results of this modelling study imply that an increased heat input at the base of the crust followed by convective transport of heat upward is required to explain the geophysical and petrological evidence for extensive crustal melting beneath the Altiplano–Puna plateau. The preferred scenario which satisfies the timing and nature of magmatism and the geophysical constraints is a combination of convective heat and mass transfer from hot, partially molten lower crust with intrusion of arc magmas into the mid-crust. Convection by bulk flow of hot crustal material heats the mid-crust most efficiently. Such convection is possible when the middle and lower crust are mechanically weak (quartz dominated rheology), the basal heat flow from the mantle is high (>60 mW/m^2) and tectonic shortening is active. The convection raises ambient temperatures in the mid-crust to near solidus conditions, and the addition of heat and fluid from trapped arc andesite magmas intensify extensive partial melting and may also enhance magma transport to the surface.

Acknowledgements

This study is a part of the collaborative project SFB-267, Deformation in Central Andes, funded by the Deutsche Forschungsgemeinschaft. The work of A.B. was supported by the Alexander-von-Humboldt Foundation and the GeoForschungs-Zentrum Potsdam. We gratefully acknowledge the contribution of Alexey Poliakov, who provided the original version of the numeric code, Yuri Podladchikov, Sergey Medvedev and an anonymous reviewer who provided constructive and stimulating reviews as well as useful collaboration with Alexander Gliko and members of the SFB-267 team. *[RV]*

Appendix

The numerical algorithm employed in this study solves the following system of coupled thermo-mechanical equations in 2-D.

Momentum conservation equation:

$$\rho_{\text{inert}}\frac{\partial v_i}{\partial t} = -\frac{\partial p}{\partial x_i} + \frac{\partial \tau_{ij}}{\partial x_j} + \rho g_i,\ i = 1,2 \qquad (1)$$

Mass conservation and constitutive laws:

$$\frac{\partial p}{\partial t} = -K\frac{\partial v_i}{\partial x_i},\ \frac{\partial \varepsilon_{ij}}{\partial t} = \frac{1}{2G}\frac{\partial \tau_{ij}}{\partial t} + \frac{1}{2\eta}\tau_{ij} \quad (2)$$

or Mohr–Coloumb elasto-plasticity with zero dilation.

And energy conservation equation:

$$\rho C_p \frac{\partial T}{\partial t} = \frac{\partial}{\partial x_i}(\lambda \frac{\partial T}{\partial x_i}) + 2\dot{\varepsilon}_{II}\tau_{II} + \rho A + \rho L\frac{\partial \xi}{\partial t} \quad (3)$$

Here ρ_{inert} is inertial density, x_i are coordinates, t is time, v_i is velocity, p is pressure, τ_{ij} and ε_{ij} are stress and strain deviators, ρ is density, g_i is gravity vector, K and G are bulk and shear moduli, η non-Newtonian power-law viscosity $\eta = (1/2)B^{-1/n}(\dot{\varepsilon}_{II})^{1/n-1}\exp(E_a/(nRT))$, B, n, E_a are parameters, $\dot{\varepsilon}_{II}$, τ_{II} are second invariants of strain rate and stress deviators, R is gas constant, C_p is heat capacity, T is temperature, λ is heat conductivity, A is radioactive heat production, L is latent heat of fusion and ξ is melt fraction.

As constitutive laws, we employ both Mohr–Coloumb elasto-plasticity with softening and Maxwell visco-elasticity with non-Newtonian power-law viscosity. Viscosity is limited from below by $\eta_{min} = 10^{17}$ Pa s. Material parameters are listed in Table 1. The system of equations is integrated in time by an explicit, time-marching scheme on a Lagrangian grid [25]. This algorithm uses a technical 'trick' by including a pseudo-inertial term in the momentum equation (left-side term in Eq. 1) to allow for explicit integration of velocities. The value of this term has to be small enough not to affect computation results, and is controlled by a characteristic Reynolds number $\mathrm{Re} = \rho_{inert} vL/\eta$, where v and L stand for characteristic flow velocity and length, η is viscosity [25]. This number represents the relative role of inertial forces in the system. It is dealt with

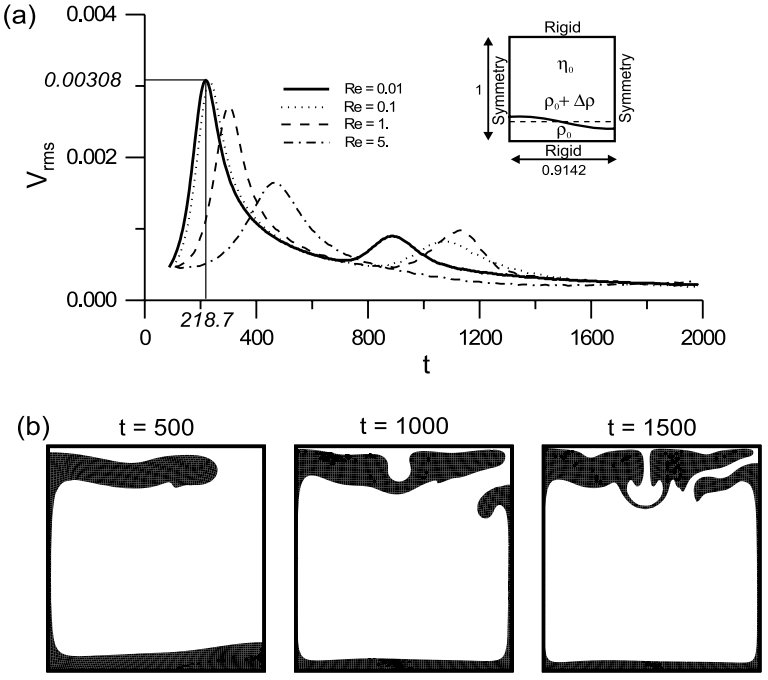

Fig. A1. Results of modelling Rayleigh–Taylor instability in an isoviscous medium using model design and parameters following van Keken et al. [50] (benchmark test). Grid resolution is 100×100 elements. (a) Non-dimensional root mean square velocities (Vrms) versus non-dimensional time in model runs with different Reynolds numbers Re. Compare with figure 3a in [50]. Inset shows the model design. (b) Evolution of instability with time. Compare with figure 2 in [50].

via so-called inertial density (ρ_{inert}), which is also a parameter that controls the time step of calculations. Thus, too high a value of inertial density corresponds to a large time step, but leads to a high Re number and, hence, to computation damping of the fastest motions. On the other hand, too low an inertial density leads to an undamped solution, but requires too small (computationally prohibitive) time steps.

In order to calibrate this method and to check the efficiency of our modified code to calculate large deformations we have performed a series of benchmark tests by modelling a Rayleigh–Taylor instability following the benchmark study by van Keken et al. [50]. Fig. A1 presents model description and test results. We obtained a very good solution for $Re = 10^{-2}$ (compare figures 2 and 3a from [50]). Solutions remain reasonably good at $Re = 10^{-1}$, but become increasingly damped at larger Reynolds numbers as found in the previous study [25].

Based on these results we performed our model calculations while trying to keep $Re < 10^{-2}$. If, however, the time step became too small, as in the case of intensive convection, a minimal time step of 1 yr was fixed instead of Re, and the resulting values of Re were monitored. In all calculations without intensive convection, the condition of $Re < 10^{-2}$ is fulfilled. In the models with intensive convection, the Reynolds numbers increased to as high as 10^{-1} or even 1. In these cases convection was significantly damped and the calculation results should be considered as conservative.

In our modelling we consider effect of melt segregation and removal as follows. When accumulated melt in the lower crust exceeds the so-called second percolation threshold [43] (here set at 25%), we begin removing melt by small portions at each time step and repositioning it into the mid-crust at 20–25 km. This process of removal/emplacement is continued until the melt fraction in the lower crustal reservoir drops to the first percolation threshold (10%), which takes some 10^3 years (i.e., very fast relative to deformation). An explicit integration scheme allows us to handle large local volume changes associated with this processes, which is very difficult in implicit integration schemes.

References

[1] B.L. Isacks, Uplift of the Central Andean Plateau and bending of the Bolivian Orocline, J. Geophys. Res. 93 (1988) 3211–3231.
[2] R.W. Allmendinger, T.E. Jordan, S.M. Kay, B.L. Isacks, The evolution of the Altiplano-Puna plateau of the central Andes, Annu. Rev. Earth Planet. Sci. 25 (1997) 139–174.
[3] S.L. de Silva, Altiplano-Puna volcanic complex of the central Andes, Geology 17 (1989) 1102–1106.
[4] P.W. Francis, R.S.J. Sparks, C.J. Hawkesworth, R.S. Thorpe, D.M. Pyle, S.R. Tait, M.S. Mantovani, F. McDermott, Petrology and geochemistry of volcanic rocks of the Cerro Galán caldera, northwest Argentina, Geol. Mag. 126 (1989) 515–547.
[5] M.H. Ort, B.L. Coira, M.M. Mazzoni, Generation of a crust-mantle magma mixture: magma sources and contamination at Cerro Panizos, Central Andes, Contrib. Mineral. Petrol. 123 (1996) 308–322.
[6] B. Coira, J. Davidson, C. Mpodozis, V. Ramos, Tectonic and magmatic evolution of the Andes of northern Argentina and Chile, Earth Sci. Rev. 18 (1982) 303–322.
[7] A.K. Schmitt, S.L. de Silva, R.B. Trumbull, R. Emmermann, Magma evolution in the Purico ignimbrite complex, northern Chile: evidence for zoning of a dacitic magma by injection of rhyolitic melts following mafic recharge, Contrib. Mineral. Petrol. 140 (2001) 680–700.
[8] X. Yuan, S.V. Sobolev, R. Kind, O. Oncken et al., Subduction and collision processes in the Central Andes constrained by converted seismic phases, Nature 408 (2000) 958–961.
[9] J. Chmielowski, G. Zandt, C. Haberland, The Central Andean Altiplano-Puna magma body, Geophys. Res. Lett. 26 (1999) 783–786.
[10] J. Lindsay, A.K. Schmitt, R.B. Trumbull, S.L. deSilva, W. Siebel, R. Emmermann, Magmatic evolution of the La Pacana caldera system, Central Andes: Compositional variation of two cogenetic, large-volume felsic ignimbrites, J. Petrol. 42 (2000) 459–486.
[11] M. Schmitz, W.-D. Heinsohn, F.R. Schilling, Seismic, gravity and petrological evidence for partial melt beneath the thickened Central Andean Crust (21–23°S), Tectonophysics 270 (1997) 313–326.
[12] G.M. Partzsch, F.R. Schilling, J. Arndt, The influence of partial melting on the electrical behavior of crustal rocks laboratory examinations, model calculations and geological interpretations, Tectonophysics 317 (2000) 189–203.
[13] M. Springer, A. Förster, Heat-flow density across the Central Andean subduction zone, Tectonophysics 291 (1998) 123–139.
[14] X. Yuan, S.V. Sobolev, R. Kind, New data on Moho

topography in the Central Andes and their geodynamic implications, Earth Planet. Sci. Lett. (in press).
[15] S. Lamb, L. Hoke, L. Kennan, J. Dewey, Cenozoic evolution of the Central Andes in Bolivia and Northern Chile, in: J.P. Burg, M. Ford (Eds.), Orogeny through time, Geol. Soc. Spec. Publ. 121 (1997) 237–264.
[16] A.D. Huerta, L.H. Royden, K.V. Hodges, The thermal structure of collisional orogens as a response to accretion, erosion, and radiogenic heating, J. Geophys. Res. 103 (1998) 15287–15302.
[17] P.C. England, A. Thompson, Some thermal and tectonic models for crustal melting in continental collision zones, in: M.P. Coward, A.C. Ries (Eds.), Collision tectonics, Geol. Soc. Am. Spec. Publ. 19 (1986) 83–94.
[18] P.C. England, P. Molnar, The interpretation of inverted metamorphic isograds using simple physical calculations, Tectonics 12 (1993) 145–157.
[19] P.H. Leloup, Y. Ricard, J. Battaglia, R. Lacassin, Shear heating in continental strike-slip zones: model and field examples, Geophys. J. Int. 136 (1999) 19–40.
[20] C. Kincaid, P. Silver, The role of viscous dissipation in the orogenic process, Earth Planet. Sci. Lett. 142 (1996) 271–288.
[21] N. Laube, J. Springer, Crustal melting by ponding of mafic magmas: a numerical model, J. Volcanol. Geotherm. Res. 81 (1998) 19–35.
[22] P. Bird, Continental delamination and the Colorado Plateau, J. Geophys. Res. 84 (1979) 7561–7571.
[23] G.A. Houseman, D.P. McKenzie, P. Molnar, Convective instability of a thickened boundary layer and its relevance for the thermal evolution of continental convergent belts, J. Geophys. Res. 86 (1981) 6115–6132.
[24] R.W. Kay, S.M. Kay, Delamination and delamination magmatism, Tectonophysics 219 (1993) 177–189.
[25] A.N. Poliakov, P.A. Cundall, Y.Y. Podladchikov, V.A. Lyakhovsky, An explicit inertial method for the simulation of the viscoelastic flow: an evaluation of elastic effects on diapiric flow in two- and three-layers models, in: D.B. Stone, S.K. Runcorn (Eds.), Flow and Creep in the Solar system: Observations, Modelling and Theory, Kluwer Academic, Dordrecht, 1993, pp. 175–195.
[26] P.A. Cundall, M. Board, A microcomputer program for modelling large-strain plasticity problems, in: G. Swoboda (Ed.), Numerical Methods in Geomechanics, Balkema, Rotterdam, 1989, pp. 2101–2108.
[27] W.R. Buck, A.N. Poliakov, Abyssal hills formed by stretching oceanic lithosphere, Nature 392 (1998) 272–275.
[28] M. Gerbault, E.B. Burov, A.N. Poliakov, M. Daignieres, Do faults trigger folding in the lithosphere?, Geophys. Res. Lett. 26 (1999) 271–274.
[29] L.L. Lavier, W.R. Buck, A.N. Poliakov, Self-consistent rolling-hinge model for the evolution of large-offset low-angle normal faults, Geology 27 (1999) 1127–1130.
[30] S.V. Sobolev, A.Yu. Babeyko, Modeling of mineralogical composition, density and elastic wave velocities in anhydrous magmatic rocks, Surv. Geophys. 15 (1994) 515–544.
[31] G. Ranalli, D.C. Murphy, Rheological stratification of the lithosphere, Tectonophysics 132 (1987) 281–295.
[32] J. Arndt, T. Bartel, E. Scheuber, F. Schilling, Thermal and rheological properties of granodioritic rocks from the Central Andes, North Chile, Tectonophysics 271 (1997) 75–88.
[33] F. Lucassen, R. Becchio, R. Harmon, S. Kasemann, G. Franz, R. Trumbull, R.L. Romer, P. Dulski, Composition and density model of the continental crust in an active continental margin – the Central Andes between 18° and 27°S, Tectonophysics 341 (2001) 195–223.
[34] E-an Zen, Thermal modelling of stepwise anatexis in a thrust-thickened sialic crust, Trans. R. Soc. Edinburgh Earth Sci. 79 (1988) 223–235.
[35] K.J.W. McCaffrey, N. Petford, Are granitic intrusions scale invariant?, J. Geol. Soc. London 154 (1997) 1–4.
[36] S.L. de Silva, J.P. Davidson, I.W. Croudace, A. Escobar, Volcanological and petrological evolution of Volcan Tata Sabaya, SW Bolivia, J. Volcanol. Geotherm. Res. 55 (1993) 305–335.
[37] T.C. Feeley, J. Davidson, Petrology of calc-alkaline lavas at Volcan Ollagüe and the origin of compositional diversity at Central Andean stratovolcanoes, J. Petrol. 35 (1994) 1295–1340.
[38] S.J. Matthews, R.S.J. Sparks, M.C. Gardeweg, The Piedras Grandes-Soncor eruptions, Lascar Volcano, Chile: evolution of a zoned magma chamber in the Central Andes, J. Petrol. 40 (1999) 1891–1919.
[39] P.W. Francis, C.J. Hawkesworth, Late Cenozoic rates of magmatic activity in the Central Andes and their relationships to continental crust formation and thickening, J. Geol. Soc. London 151 (1994) 845–854.
[40] A. Reymer, G. Schubert, Phanerozoic addition rates to the continental crust and continental growth, Tectonics 3 (1984) 63–77.
[41] W.S. Holbrook, D. Lizarralde, S. McGeary, N. Bangs, J. Diebold, Structure and composition of the Aleutian island arc and implications for continental crustal growth, Geology 27 (1999) 31–34.
[42] V. Gardien, A.B. Thompson, D. Grujic, P. Ulmer, Experimental melting of biotite + plagioclase + quartz ± muscovite assemblages and implications for crustal melting, J. Geophys. Res. 100 (1995) 15581–15591.
[43] J.-L. Vigneresse, P. Barbey, M. Cuney, Rheological transitions during partial melting and crystallisation with application to felsic magma segregation and transfer, J. Petrol. 37 (1996) 1579–1600.
[44] N. Petford, A.R. Cruden, K.J.W. McCaffrey, J.-L. Vigneresse, Granite magma formation, transport and emplacement in the Earth's crust, Nature 408 (2000) 669–673.
[45] D. Bittner, H. Schmeling, Numerical modelling of melting processes and induced diapirism in the lower crust, Geophys. J. Int. 123 (1995) 59–70.
[46] M. Springer, Interpretation of heat-flow density in the Central Andes, Tectonophysics 306 (1999) 377–395.
[47] L.L. Perchuk, Y.Y. Podladchikov, A.N. Poliakov, P-T

paths and geodynamic modeling of some metamorphic processes, J. Metamorph. Geol. 10 (1992) 311–319.
[48] F. Lucassen, S. Lewerenz, G. Franz, J. Viramonte, K. Mezger, Metamorphism, isotopic ages and composition of lower crustal granulite xenoliths from the Cretaceous Salta Rift, Argentina, Contrib. Mineral. Petrol. 134 (1999) 325–341.
[49] M.R. Handy, S. Wissing, J.E. Streit, Strength and structure of mylonite with combined frictional-viscous rheology and varied bimineralic composition, Tectonophysics 303 (1999) 175–192.
[50] P.E. vanKeken, S.D. King, H. Schmeling, U.R. Christensen, D. Neumeister, M.-P. Doin, A comparison of methods for the modeling of thermochemical convection, J. Geophys. Res. 102 (1997) 22477–22495.